JACS
JOURNAL OF THE AMERICAN CHEMICAL SOCIETY
Article
pubs.acs.org/JACS

Control of Grafting Density and Distribution in Graft Polymers by Living Ring-Opening Metathesis Copolymerization

Tzu-Pin Lin,[†] Alice B. Chang,[†] Hsiang-Yun Chen,[†] Allegra L. Liberman-Martin,[†] Christopher M. Bates,[‡,⊥] Matthew J. Voegtle,[§] Christina A. Bauer,[§] and Robert H. Grubbs*[,†]

[†]Division of Chemistry and Chemical Engineering, California Institute of Technology, Pasadena, California 91125, United States
[‡]Materials Department and [⊥]Department of Chemical Engineering, University of California, Santa Barbara, California 93106, United States
[§]Department of Chemistry, Whittier College, Whittier, California 90608, United States

Supporting Information

ABSTRACT: Control over polymer sequence and architecture is crucial to both understanding structure–property relationships and designing functional materials. In pursuit of these goals, we developed a new synthetic approach that enables facile manipulation of the density and distribution of grafts in polymers via living ring-opening metathesis polymerization (ROMP). Discrete *endo*,*exo*-norbornenyl dialkylesters (dimethyl **DME**, diethyl **DEE**, di-*n*-butyl **DBE**) were strategically designed to copolymerize with a norbornene-functionalized polystyrene (**PS**), polylactide (**PLA**), or polydimethylsiloxane (**PDMS**) macromonomer mediated by the third-generation metathesis catalyst (**G3**). The small-molecule diesters act as diluents that increase the average distance between grafted side chains, generating polymers with variable grafting density. The grafting density (number of side chains/number of norbornene backbone repeats) could be straightforwardly controlled by the macromonomer/diluent feed ratio. To gain insight into the copolymer sequence and architecture, self-propagation and cross-propagation rate constants were determined according to a terminal copolymerization model. These kinetic analyses suggest that copolymerizing a macromonomer/diluent pair with evenly matched self-propagation rate constants favors randomly distributed side chains. As the disparity between macromonomer and diluent homopolymerization rates increases, the reactivity ratios depart from unity, leading to an increase in gradient tendency. To demonstrate the effectiveness of our method, an array of monodisperse polymers (**PLA**^{x}-*ran*-**DME**$^{1-x}$)$_n$ bearing variable grafting densities (x = 1.0, 0.75, 0.5, 0.25) and total backbone degrees of polymerization (n = 167, 133, 100, 67, 33) were synthesized. The approach disclosed in this work therefore constitutes a powerful strategy for the synthesis of polymers spanning the linear-to-bottlebrush regimes with controlled grafting density and side chain distribution, molecular attributes that dictate micro- and macroscopic properties.

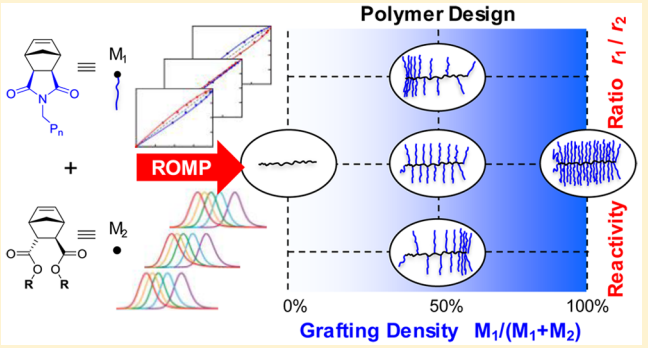

INTRODUCTION

Bottlebrush polymers are a subset of graft polymers that consist of a polymer backbone bearing densely grafted side chains.[1] The steric demands exerted by the side chains encourage the backbone to adopt an extended wormlike conformation,[2] rendering distinct mechanical and physical features uncharacteristic of linear analogues.[3] Numerous studies have accordingly leveraged the unique attributes of bottlebrush polymers to address challenges in diverse applications including drug delivery,[4] surface coatings,[5] photolithography,[6] pressure sensors,[7] transport,[8] energy storage,[9] and photonics.[10] These achievements are crucially facilitated by a host of grafting-to, grafting-from, and grafting-through polymerization methodologies, enabling control over structural parameters such as the backbone degree of polymerization, side chain degree of polymerization, molar mass dispersity, and chemical functionality.

Despite these advances, systematic variation of grafting density exhaustively spanning the linear-to-bottlebrush regimes remains synthetically challenging.[11] As recently highlighted, grafting density is of fundamental importance in shaping the mechanical[12]/physical[13] properties, self-assembly,[14] and stimuli-responsiveness[15] exhibited by graft polymers. We therefore anticipate that developing an effective and efficient synthetic protocol to modify grafting density will be vital in deepening understanding of the structure–property–function relationships[16] in graft polymers. Toward this goal, Matyjaszewski has previously reported the copolymerization of an acryloyl-

Received: January 23, 2017
Published: February 21, 2017

DOI: 10.1021/jacs.7b00791
J. Am. Chem. Soc. 2017, 139, 3896–3903

functionalized macromonomer with *n*-butyl acrylate using atom transfer radical polymerization (ATRP).[17] This work elegantly illustrated the role of *n*-butyl acrylate as a diluent that served to increase the average distance between grafting points. However, harsh conditions and prolonged reaction times were required, and only low backbone degrees of polymerization could be achieved at high grafting density due to the steric profile of the macromonomers. Another method described by Kamigaito employed radical copolymerization of limonene and maleimide derivatives, generating an ABB alternating propagation sequence.[18] The limonene or maleimide derivative was selectively functionalized to subsequently enable a "grafting-from" installation of poly(methyl methacrylate) side chains. However, this system could only yield polymers with precisely 33% or 67% grafting densities. Also, high molar mass dispersity ($Đ \approx 1.7$) was observed with this method.

Inspired by these earlier results, we began investigating living ring-opening metathesis polymerization (ROMP)[19] as another approach that could potentially circumvent the aforementioned challenges. Our method harnesses the many advantages of living ROMP including (1) mild reaction conditions, (2) low molar mass dispersity, (3) uniform side chain lengths, (4) living character with tunable backbone degrees of polymerization, and (5) functional group tolerance. We herein provide the first illustration that ROMP can be exploited in the context of grafting density control. Monodisperse polymers with grafting densities spanning the linear, comb, and bottlebrush regimes are easily accessible by copolymerization reactions of a norbornene-functionalized macromonomer with a discrete small-molecule diluent in different feed ratios (Chart 1). In-depth kinetic analyses reveal that the distribution (random or gradient) of grafts can be adjusted by simple modifications to the diluent ester substituents. Living ROMP therefore constitutes an effective strategy in controlling polymer architecture,[20] providing new opportunities for polymer design and applications.

Chart 1. Grafting Density and Side Chain Distribution Control via Ring-Opening Metathesis Polymerization (ROMP)

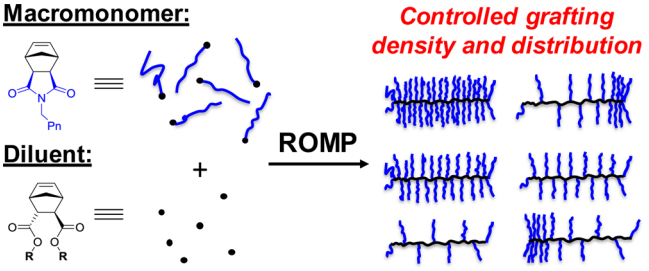

RESULTS AND DISCUSSION

Monomer Design. In pursuit of this approach, we launched investigation into the homopolymerization kinetics of macromonomers and diluents bearing polymerizable end groups. We avoided cyclic olefinic monomers that inherently favor alternating sequences,[21] since strict alternation would only afford 50% grafting density and preclude control over graft distribution. Instead, norbornene-functionalized derivatives, which rarely result in alternating polynorbornene,[22] were selected for the present study. Relief of the high ring strain in norbornene, mediated by highly active ruthenium metathesis catalysts, enables grafting-through ROMP to produce well-defined bottlebrush polymers.[23] We also note that random copolymerization of norbornenes has been previously inferred,[23b,24] suggesting potential opportunities for advanced sequence control. However, quantitative sequence determination has been lacking. With this context in mind, *ω*-norbornenyl polystyrene (**PS**, M_n = 3990 g/mol), polylactide (**PLA**, M_n = 3230 g/mol), and polydimethylsiloxane (**PDMS**, M_n = 1280 g/mol) macromonomers featuring an *exo,exo*-imide anchor group were prepared (Figure 1). **PS** and **PLA** macromonomers of similar molar masses have been previously employed in the synthesis of well-defined bottlebrush polymers and were therefore attractive candidates for our studies.[9,10] For the diluents, we were drawn to a family of racemic *endo,exo*-norbornenyl diesters (dimethyl **DME**, diethyl **DEE**, and di-*n*-butyl **DBE**, each with molar mass <300 g/mol) which could be easily assembled by Diels–Alder reactions of cyclopentadiene with the corresponding fumarate. We anticipated different propagation rates for these norbornenyl diesters,[25] amenable to tuning the relative reactivity of diverse diluent/macromonomer pairs.

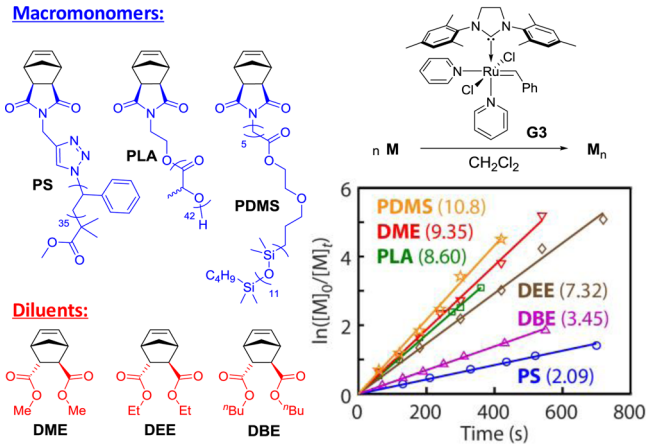

Figure 1. Left: Structures of macromonomers (**PS**, **PLA**, **PDMS**) and diluents (**DME**, **DEE**, **DBE**). Right: Plots of $\ln([M]_0/[M]_t)$ versus time, showing first-order kinetics for the homopolymerization of norbornene monomers (0.05 M) catalyzed by **G3** (0.5 mM) in CH_2Cl_2 at 298 K (orange stars, **PDMS**; inverted red triangles, **DME**; green squares, **PLA**; brown diamonds, **DEE**; purple triangles, **DBE**; blue circles, **PS**). The numbers in parentheses represent the values of k_{obs} (10^{-3} s^{-1}) under the reaction conditions.

Homopolymerization Kinetics. ROMP of each monomer in CH_2Cl_2 (0.05 M) was mediated by the highly active third-generation olefin metathesis catalyst,[26] $(H_2IMes)(pyr)_2(Cl)_2$-Ru=CHPh (**G3**, 0.5 mM). At different time points, aliquots were extracted from the reaction mixture and immediately quenched in separate vials containing a large excess of ethyl vinyl ether. Subsequently, the quenched reactions were analyzed by size-exclusion chromatography (SEC) and ^{1}H NMR spectroscopy, allowing evaluation of the conversion, molar mass, and molar mass dispersity. As shown in Figure 1, the depletion of monomers is first-order. Since the rate of initiation for **G3** is much faster than that of propagation under these conditions,[26,27] the observed first-order rate constant (k_{obs}) can be used to calculate the second-order self-propagation rate constant (k_{homo}) according to eq 1 (M = monomer):

DOI: 10.1021/jacs.7b00791
J. Am. Chem. Soc. 2017, 139, 3896–3903

$$-\frac{d[M]_t}{dt} = k_{obs}[M]_t = k_{homo}[\mathbf{G3}]_0[M]_t \quad (1)$$

The k_{homo}, which is independent of the catalyst concentration, is of direct relevance to our copolymerization kinetic analyses (*vide infra*). The homopolymerization kinetic results are summarized in Table 1. Comparing the three macromonomers,

Table 1. Homopolymerization Reactions of CH_2Cl_2 at 298 K

		M_n (kg/mol)			
monomer	k_{homo} (M^{-1} s^{-1})	expected[a]	measured[b]	$Đ$[b]	conv. (%)
PS	4.18	399	375	1.06	94[c]
PLA	17.2	323	319	1.01	99[c]
PDMS	21.6	128	131	1.02	99[c]
DME	18.7	21.0	21.7	1.02	100[d]
DEE	14.6	23.8	24.2	1.02	100[d]
DBE	6.90	29.4	29.6	1.02	100[d]

[a]Based on the monomer/**G3** ratio of 100/1. [b]Determined by SEC light scattering detector. [c]Determined by SEC differential refractive index detector. [d]Determined by ^{1}H NMR.

PDMS possesses the largest k_{homo} of 21.6 M^{-1} s^{-1}. The k_{homo} of **PLA** (17.2 M^{-1} s^{-1}) is around four times as large as that measured for **PS** (4.18 M^{-1} s^{-1}), in line with previous observations.[23b] The k_{homo} values of the norbornenyl diesters trends inversely with the bulkiness of the ester substituents as anticipated. Indeed, the k_{homo} measured for **DME** (18.7 M^{-1} s^{-1}) is larger than that of **DEE** (14.6 M^{-1} s^{-1}) or **DBE** (6.90 M^{-1} s^{-1}). Collectively, these results reinforce that the norbornene monomer sterics play an important role in the rate of ROMP.

Analytical Methods for Copolymerization Kinetics. The homopolymerization kinetic analyses indicate that ROMP of each individual macromonomer or diluent is well-behaved. However, controlling side chain density and distribution also requires knowledge of the macromonomer/diluent copolymerization kinetics. To this end, we investigated copolymerization reactions based on the Mayo–Lewis terminal model[28] (Scheme 1) in which the reactivity of two distinct propagating species (hereafter denoted as M_1* and M_2*) strictly depends on the monomer at the growing chain end. In other words, the chemical reactivity of the Ru catalyst was assumed to be primarily influenced by the electronic/steric properties of the latest-formed alkylidene. The copolymerization of M_1 (macromonomer) and M_2 (diluent) can be described by four unique propagation reactions with individual rate constants k_{11}, k_{12}, k_{21}, and k_{22}. The reactivity ratios ($r_1 = k_{11}/k_{12}$, $r_2 = k_{22}/k_{21}$) are defined as the tendency for the propagating species to react with the same monomer over the other. As depicted in Scheme 1, the copolymerization is inherently directed by the reactivity ratios, leading to sequences such as alternating, blocky, random, or gradient.

Historically, a number of methodologies have been established to determine the reactivity ratios for copolymerizations. Popular techniques include those pioneered by Mayo–Lewis,[28] Fineman–Ross,[29] and Kelen–Tüdös,[30] among others.[31] While these linear regression methods bear irrefutable merit, they are derived from equations based on the steady-state approximation, with the assumption that the rates of crossover are identical, i.e., $k_{12}[M_1^*]_t[M_2]_t = k_{21}[M_2^*]_t[M_1]_t$. As such, these methods are only applicable under steady-state conditions in which the change in monomer feed is insignificant.[32] Obtaining kinetic data in the required low-conversion regime is analytically more challenging for fast polymerization reactions such as **G3**-mediated ROMP.

Scheme 1. Terminal Model Describing the Copolymerization of M_1 and M_2

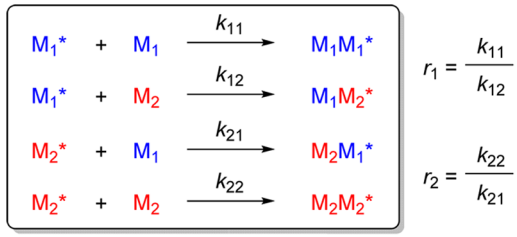

Case I: r_1, r_2 << 1 (alternating)

$M_1M_2M_1M_2M_1M_2M_1M_2M_1M_2M_1M_2M_1M_2M_1M_2M_1M_2M_1M_2$

Case II: r_1, r_2 >> 1 (blocky)

$M_1M_1M_1M_1M_1M_1M_1M_1M_1M_1M_2M_2M_2M_2M_2M_2M_2M_2M_2M_2$

Case III: $r_1 = r_2 = 1$ (random)

$M_2M_2M_1M_2M_1M_1M_1M_2M_1M_2M_1M_2M_2M_1M_1M_2M_1M_2M_2M_1$

Case IV: $r_1 < 1 < r_2$ (gradient)

$M_2M_2M_2M_2M_1M_2M_2M_2M_1M_1M_1M_2M_2M_1M_1M_1M_2M_1M_1M_1M_1$

Given the aforementioned constraint, we developed another approach that bypasses the steady-state approximation. According to the terminal model, the time-dependent concentrations of M_1, M_2, M_1*, and M_2* can be described by the following ordinary differential equations:

$$-\frac{d[M_1]_t}{dt} = k_{11}[M_1^*]_t[M_1]_t + k_{21}[M_2^*]_t[M_1]_t \quad (2)$$

$$-\frac{d[M_2]_t}{dt} = k_{12}[M_1^*]_t[M_2]_t + k_{22}[M_2^*]_t[M_2]_t \quad (3)$$

$$-\frac{d[M_1^*]_t}{dt} = k_{12}[M_1^*]_t[M_2]_t - k_{21}[M_2^*]_t[M_1]_t \quad (4)$$

$$-\frac{d[M_2^*]_t}{dt} = k_{21}[M_2^*]_t[M_1]_t - k_{12}[M_1^*]_t[M_2]_t \quad (5)$$

While the exact analytical solutions for eqs 2–5 cannot be obtained, numerical solutions for $[M_1]_t$, $[M_2]_t$, $[M_1^*]_t$, and $[M_2^*]_t$ can be generated if the propagation rate constants are provided. In our study, the homopolymerization rate constants k_{11} and k_{22} can be independently measured (see Table 1). Further, the instantaneous monomer concentrations $[M_1]_t$ and $[M_2]_t$ during the copolymerization can be determined by the ethyl vinyl ether quenching method. In living ROMP, the sum of $[M_1^*]_t$ and $[M_2^*]_t$ should be $[\mathbf{G3}]_0$. Taken collectively, the best numerical solutions for k_{12} and k_{21} for eqs 2–5 can be determined using a nonlinear least-squares curve fitting method (see Supporting Information (SI) for the MATLAB codes).

Copolymerization Kinetics. We first investigated the copolymerization of **PS** (0.05 M) and **DME** (0.05 M) mediated by **G3** (0.5 mM) in CH_2Cl_2 (Figure 2). The conditions, including the monomer and catalyst concentrations, were identical to those employed in homopolymerization reactions. Aliquots were extracted at different time points, quenched, and subjected to SEC and NMR analyses. The SEC

DOI: 10.1021/jacs.7b00791
J. Am. Chem. Soc. 2017, 139, 3896–3903

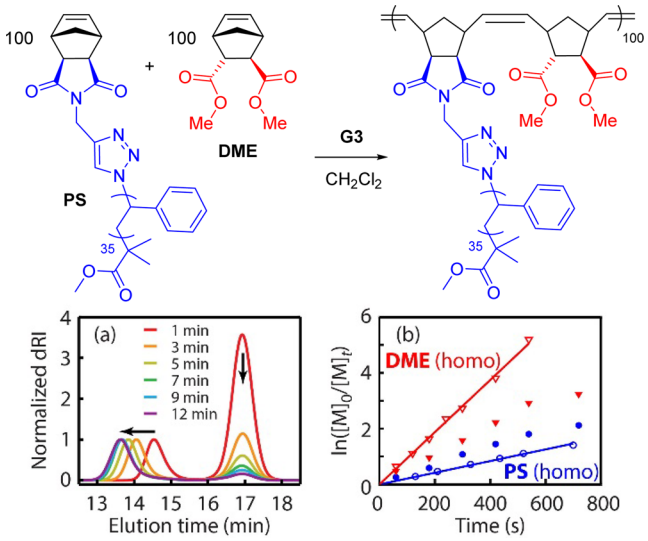

Figure 2. Copolymerization of **PS** (0.05 M) and **DME** (0.05 M) catalyzed by **G3** (0.5 mM) in CH_2Cl_2 at 298 K. (a) Normalized differential refractive index (dRI) traces from size-exclusion chromatography. (b) Plots of $\ln([M]_0/[M]_t)$ versus time as monitored by ^{1}H NMR spectroscopy (filled blue circles, **PS**; filled red triangles, **DME**). Unfilled blue circles (**PS**), unfilled red triangles (**DME**), and the solid lines, plotted for comparison, were obtained from homopolymerization reactions under the same conditions.

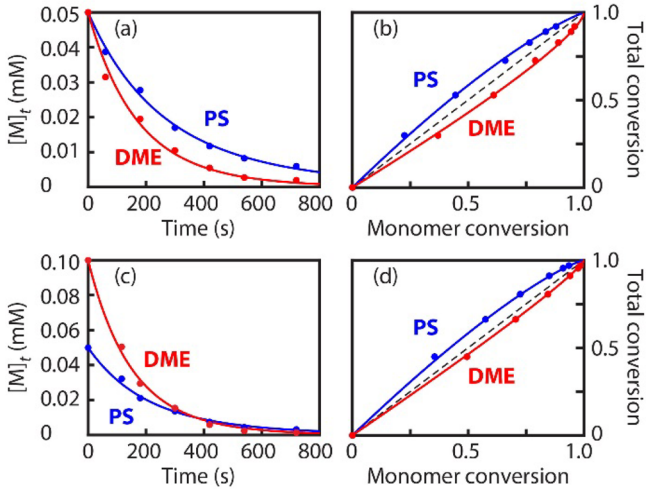

Figure 3. Nonlinear least-squares curve fitting for the copolymerization of (a,b) **PS** (0.05 M) and **DME** (0.05 M) and (c,d) **PS** (0.05 M) **DME** (0.10 M) in CH_2Cl_2 at 298 K. $[\mathbf{G3}]_0$ = 0.5 mM. Calculated fits (solid lines) show close agreement with the measured values (points). In (b) and (d), the dashed lines, included for comparison, indicate ideal random copolymerization ($r_1 = r_2 = 1$).

traces indicated the continuing depletion of **PS** as well as the concomitant growth of the copolymer (Figure 2a). In addition, the instantaneous concentrations of both monomers could be determined by ^{1}H NMR integration of their distinct norbornenyl olefinic resonances. Plotting $\ln([M]_0/[M]_t)$ as a function of time (Figure 2b) suggested that the decay of **PS** and **DME** approached *pseudo* first order. However, we note that the first order kinetics are only strictly applicable in the event that both $[M_1^*]_t$ and $[M_2^*]_t$ are constant (see eqs 2 and 3). With the same **G3** concentration of 0.5 mM, the propagation rates for **PS** and **DME** in the copolymerization reaction were, respectively, faster and slower than those measured independently in the homopolymerization reactions (Figure 2b). The increase in the rates of **PS** consumption in the copolymerization reaction could be attributed to cross-propagation being faster than self-propagation. Interestingly, the opposite trend was observed for **DME**.

To gain more insight, the kinetic profile of the copolymerization of **PS** and **DME** (1:1) was fitted to the terminal model using our analytical methods with known values of $k_{PS\text{-}PS}$, $k_{DME\text{-}DME}$, $[\mathbf{PS}]_0$, $[\mathbf{DME}]_0$, and $[\mathbf{G3}]_0$ (Figure 3a). The calculated curves of monomer conversion versus total conversion agreed satisfactorily with the experimental data (Figure 3b). This analysis generated $k_{PS\text{-}DME}$ and $k_{DME\text{-}PS}$ values of 7.74 and 13.2 M^{-1} s^{-1}, respectively (Table 2, entry 1). The reactivity ratios (r_{PS} = 0.54, r_{DME} = 1.41) indicate gradient copolymerization and can be used in the simulation of instantaneous copolymer composition (*vide infra*). Copolymerizing **PS** and **DME** in a 1:1 feed ratio could therefore be expected to yield a polymer bearing 50% grafting density and a gradient distribution of **PS** side chains. In order to further examine the validity of our methods, the copolymerization of **PS** and **DME** in a 1:2 feed ratio was carried out and subjected to the same analyses (Figure 3c,d), yielding comparable $k_{PS\text{-}DME}$ and $k_{DME\text{-}PS}$ values (Table 2, entry 2). As such, these experiments underlined the ability of the terminal model to capture the copolymerization kinetics of **G3**-catalyzed ROMP.

We next examined the 1:1 copolymerization of **PS** and **DEE** (Figure 4a, b). The measured $k_{PS\text{-}DEE}$ (7.73 M^{-1} s^{-1}, Table 2, entry 3) is very close to $k_{PS\text{-}DME}$ (7.58−7.74 M^{-1} s^{-1}), thus indicating similar chemical reactivity of the propagating species **PS*** toward **DME** and **DEE**. In sharp contrast, $k_{DEE\text{-}PS}$ (8.75 M^{-1} s^{-1}) is notably smaller than $k_{DME\text{-}PS}$ (13.2−14.6 M^{-1} s^{-1}). This observation suggests that the **PS*** alkylidene steric/electronic effects are important in governing the rate of ROMP (perhaps more so than that of the approaching norbornenyl diester). The calculated reactivity ratios r_{PS} (0.54) and r_{DEE} (1.67) indicate gradient copolymerization. In addition, the $r_{PS}r_{DEE}$ product of 0.90 suggests an almost ideal copolymerization process in which each propagating species, **PS*** and **DEE***, has the same preference for **PS** over **DEE**, i.e., $k_{PS\text{-}PS}/k_{PS\text{-}DME} \approx k_{DME\text{-}PS}/k_{DME\text{-}DME}$. The copolymerizations of **PS** and **DBE** in a 1:1 (Figure 4c,d) and 3:1 (see SI) stoichiometry have also been examined. The propagation rate constants obtained from these experiments parallel each other (Table 2, entries 4 and 5), again reflecting the competence of our analytical methods. The **PS**/**DBE** copolymerization is best described as near-ideal, approaching random, as evidenced by the reactivity ratios (r_{PS} = 0.8, r_{DBE} = 1.16−1.22) as well as their product ($r_{PS}r_{DBE}$ = 0.93−0.97).

For studies and applications in which uniform grafting density is desired, the ability to access random copolymers is crucial. The copolymerization reactions of **PS** with diluents imply that random copolymerization ($r_1 \approx r_2 \approx 1$) might be achieved when both self-propagation rate constants are similar ($k_{11} \approx k_{22}$). To examine this hypothesis, we turned our attention to the copolymerization of **PLA** (k_{homo} = 17.2 M^{-1} s^{-1}) and **DME** (k_{homo} = 18.7 M^{-1} s^{-1}). These experiments indicate that the decay of **PLA** is only marginally slower than that of **DME**, in line with an almost random copolymerization process (Figure 4e,f; Table 2, entry 6). Similarly, random copolymerization was observed for **PLA**/**DBE** (Figure 4g,h; Table 2, entry 7) as well as **PDMS**/**DME** (Figure 4i,j; Table 2, entry 8). Lastly, gradient copolymers (Table 2, entry 9, r_{PDMS} =

DOI: 10.1021/jacs.7b00791
J. Am. Chem. Soc. 2017, 139, 3896−3903

Table 2. Copolymerization Rate Constants and Reactivity Ratios in CH_2Cl_2 at 298 K

entry	M_1	M_2	$[M_1]_0$ (M)	$[M_2]_0$ (M)	k_{11} (M^{-1} s^{-1})	k_{12}[a] (M^{-1} s^{-1})	k_{22} (M^{-1} s^{-1})	k_{21}[a] (M^{-1} s^{-1})	r_1	r_2	r_1r_2
1	**PS**	**DME**	0.050	0.050	4.18	7.74	18.7	13.2	0.54	1.41	0.76
2	**PS**	**DME**	0.050	0.100	4.18	7.58	18.7	14.6	0.55	1.28	0.71
3	**PS**	**DEE**	0.050	0.050	4.18	7.73	14.6	8.75	0.54	1.67	0.90
4	**PS**	**DBE**	0.050	0.050	4.18	5.23	6.90	5.66	0.80	1.22	0.97
5	**PS**	**DBE**	0.075	0.025	4.18	5.24	6.90	5.93	0.80	1.16	0.93
6	**PLA**	**DME**	0.050	0.050	17.2	18.8	18.7	16.9	0.92	1.11	1.02
7	**PLA**	**DBE**	0.050	0.050	17.2	16.7	6.90	7.95	1.03	0.87	0.90
8	**PDMS**	**DME**	0.050	0.050	21.6	19.9	18.7	19.9	1.09	0.94	1.02
9	**PDMS**	**DBE**	0.050	0.055	21.6	19.5	6.90	15.9	1.11	0.43	0.48

[a]Obtained from least-squares curve fitting.

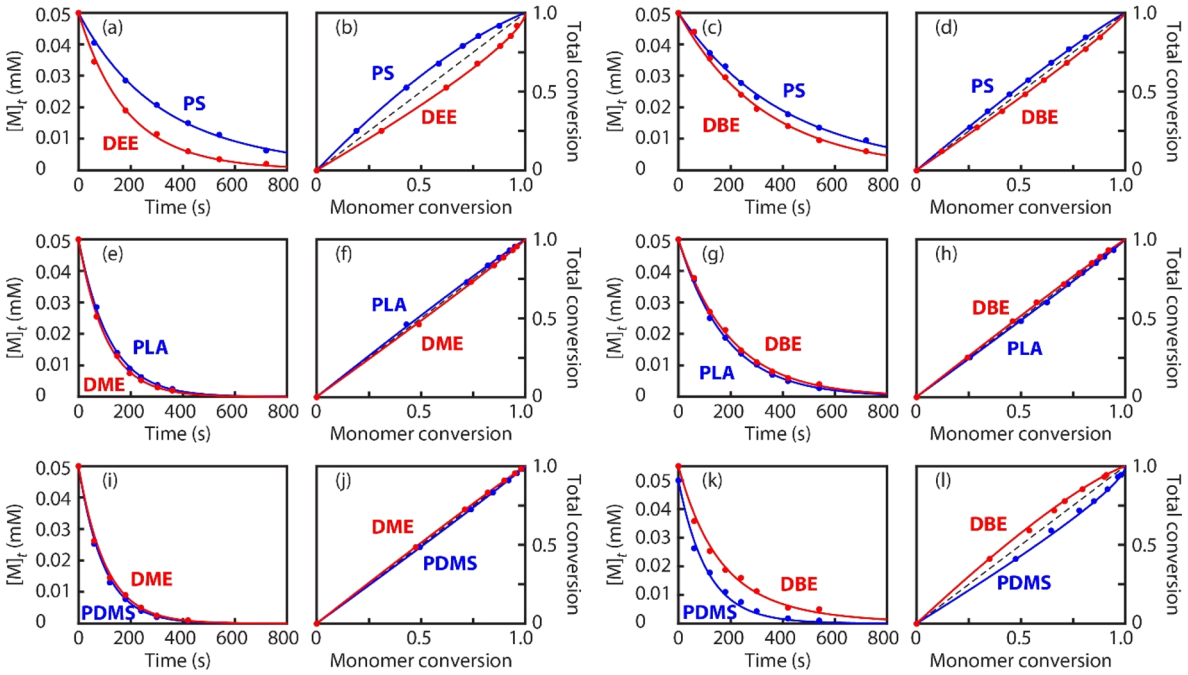

Figure 4. Nonlinear least-squares curve fitting for the copolymerization of various macromonomer/diluent pairs: (a,b) **PS**/**DEE**, (c,d) **PS**/**DBE**, (e,f) **PLA**/**DME**, (g,h) **PLA**/**DBE**, (i,j) **PDMS**/**DME**, and (k,l) **PDMS** (0.050 M)/**DBE** (0.055 M). Reaction conditions: $[M]_0$ = 0.05 M unless otherwise indicated, $[G3]_0$ = 0.5 mM, solvent = CH_2Cl_2, temperature = 298 K.

1.11, r_{DBE} = 0.43) were obtained by copolymerization reaction of **PDMS** with **DBE** (Figure 4k,l). The reactivity ratio product ($r_{PDMS}r_{DBE}$ = 0.48) indicates a departure from ideal copolymerization. This observation is seemingly correlated with the large differences in the self-propagation rate constants. Taken collectively, the copolymerization of a norbornene-functionalized macromonomer (**PS**, **PLA**, or **PDMS**) with a diluent (**DME**, **DEE**, or **DBE**) could generate either gradient or random copolymers. Kinetic analyses reveal similar k_{12} values (**PS** = 5.23−7.74 M^{-1} s^{-1}, **PLA** = 16.7−18.8 M^{-1} s^{-1}, **PDMS** = 19.5−19.9 M^{-1} s^{-1}) and disparate k_{21} values (**PS** = 5.66−14.6 M^{-1} s^{-1}, **PLA** = 7.95−16.9 M^{-1} s^{-1}, **PDMS** = 15.9−19.9 M^{-1} s^{-1}). This observation could potentially be attributed to the different steric, electronic, and ligating environments exerted by the pendant polymer group, linker, and anchor group (*exo*,*exo*-imide for macromonomer versus *endo*,*exo*-diester for diluent). The importance of the anchor group has been recently discussed by Matson in the context of self-propagation rates.[33]

Instantaneous Copolymer Composition. From the copolymerization kinetics, the rate of monomer incorporation at any given time could be calculated according to eqs 2 and 3, allowing prediction of instantaneous copolymer composition as a function of total conversion. For example, copolymerizing **PS** and **DME** in a 1:1 feed ratio results in (**PS**-*grad*-**DME**)$_n$ best described as a gradient graft polymer (Figure 5a). Such a copolymer at 100% conversion possesses, on average, 50% grafting density, i.e., one polystyrene brush per two norbornene backbone repeat units. The difference in reactivity ratios leads to richer **DME** composition at early conversion and higher **PS** incorporation toward the end. We note that similar gradient graft polymers have been previously accessed by grafting-from ATRP methods.[34] The brush distribution gradient is much less pronounced in copolymers (**PLA**-*ran*-**DME**)$_n$ (Figure 5b) and (**PDMS**-*ran*-**DME**)$_n$ (Figure 5c), in which the side chains are uniformly grafted across the entire polynorbornene backbone. Lastly, copolymerizing **PDMS**/**DBE** in a 1:1 ratio generates the gradient copolymer (**PDMS**-*grad*-**DBE**)$_n$ (Figure 5d). Unlike (**PS**-*grad*-**DME**)$_n$, our simulations indicate that (**PDMS**-*grad*-**DBE**)$_n$ is more densely grafted at early conversion. Coupled with sequential polymerization, copolymerizing **PS**/**DME** and **PDMS**/**DBE** could be exploited in the synthesis of normal tapered or inverse tapered block copolymers.[35]

Synthesis of Variable Grafting Density Polymers. To showcase the synthetic versatility of our approach, we targeted

DOI: 10.1021/jacs.7b00791
J. Am. Chem. Soc. 2017, 139, 3896−3903

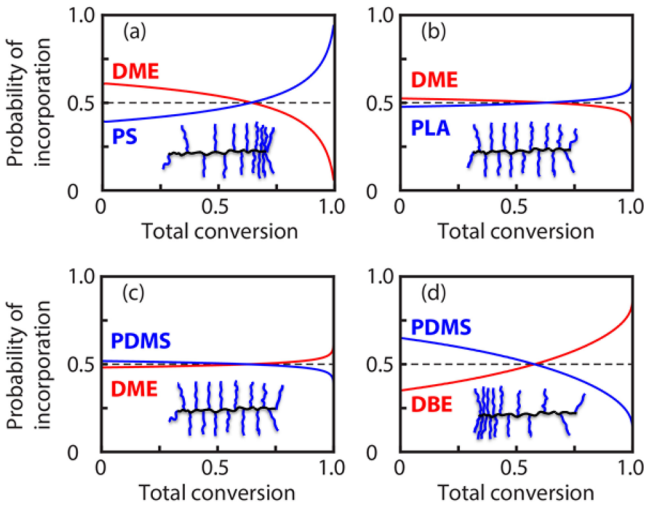

Figure 5. Simulated copolymer compositions for (a) **PS**:**DME** = 1:1, (b) **PLA**:**DME** = 1:1, (c) **PDMS**:**DME** = 1:1, and (d) **PDMS**:**DBE** = 1:1. Insets show the schematic illustrations of the corresponding polymers.

an array of polymers (**PLA**^{x}-*ran*-**DME**$^{1-x}$)$_n$ with variable grafting densities (x = 1.0, 0.75, 0.5, 0.25) and backbone lengths (n = 167, 133, 100, 67, 33). These polymers could be easily prepared by mixing **PLA**, **DME**, and **G3** in different ratios according to eqs 6 and 7 (M_1 = macromonomer, M_2 = diluent).

$$x = [M_1]_0/([M_1]_0 + [M_2]_0) \quad (6)$$

$$n = ([M_1]_0 + [M_2]_0)/[\mathbf{G3}]_0 \quad (7)$$

These copolymerization reactions were carried out under very mild conditions in CH_2Cl_2 (298 K, $[\mathbf{G3}]_0$ = 0.5 mM, 15 min), and complete monomer consumption was verified by ^{1}H NMR spectroscopy. As shown in Figure 6, the SEC analyses of the resulting polymers indicated low molar mass dispersities ($Đ$ = 1.01−1.03) as well as excellent agreement between the

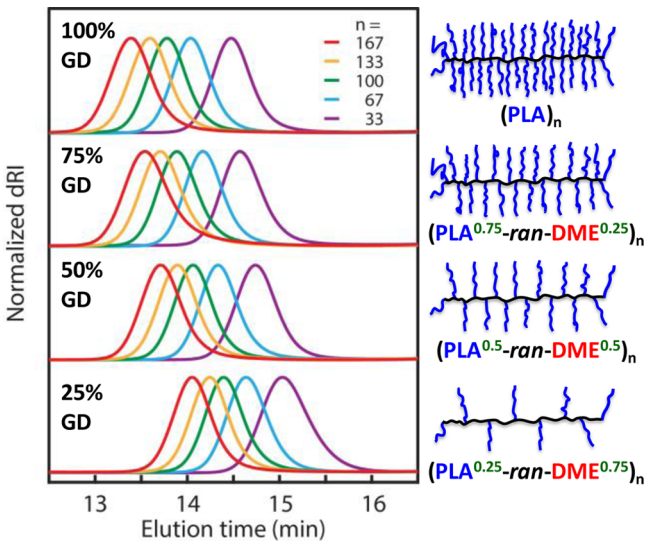

Figure 6. SEC traces of (**PLA**^{x}-*ran*-**DME**$^{1-x}$)$_n$, where x is the grafting density (1.0, 0.75, 0.5, 0.25) and n it the targeted total backbone degree of polymerization (red, 167; orange, 133; green, 100; teal, 67; purple, 33).

measured and targeted molar masses throughout the series (see SI).

Reinforcing the NMR and SEC data, differential scanning calorimetry (DSC) provided further evidence supporting the controlled incorporation of both macromonomer and diluent (see SI). For example, DSC data collected on (**PS**$^{0.5}$-*ran*-**DBE**$^{0.5}$)$_{200}$ show one glass transition temperature (T_g) at 95 °C, which lies between the T_g values of the pure components **PS**$_{100}$ (102 °C) and **DBE**$_{100}$ (71 °C).[36]

CONCLUSION

The current work introduces a general approach for simultaneously controlling the grafting density and side chain distribution of polymers. This method is achieved by ring-opening metathesis copolymerization of a norbornene-functionalized macromonomer (**PS**, **PLA**, or **PDMS**) with a discrete *endo*,*exo*-norbornenyl diester diluent (**DME**, **DEE**, or **DBE**). While such a system may appear at first glance untenable due to the vastly different steric profiles of the macromonomers and diluents, appropriate monomer design overcomes this challenge. By simple modifications to the diester substituents, the self-propagation rate constant (k_{homo}) of the diluents could be adjusted to match or mismatch those of the norbornenyl macromonomers. To investigate the copolymerization kinetics, the reaction profiles were monitored and fitted to a terminal copolymerization model using a nonlinear least-squares curve fitting method. This analysis enables close inspection of previously unexplored reactivity ratios (r_1 and r_2) as well as cross-propagation rate constants (k_{12} and k_{21}) for **G3**-catalyzed ROMP. In particular, we found that (1) copolymerizing a macromonomer/diluent pair with similar or dissimilar values of k_{homo} favors the generation of random ($r_1 \approx r_2 \approx 1$) or gradient ($r_1 < 1 < r_2$; $r_1 > 1 > r_2$) copolymers, respectively; (2) different macromonomer/diluent feed ratios could be employed to vary the grafting density from 100% to 0%; and (3) the k_{12} values measured for macromonomers (**PS** = 5.23−7.74 M^{-1} s^{-1}, **PLA** = 16.7−18.8 M^{-1} s^{-1}, **PDMS** = 19.5−19.9 M^{-1} s^{-1}) are very similar, whereas the k_{21} values are substantially different (1 = macromonomer, 2 = diluent; see Table 2), reflecting the importance of the alkylidene ligands in metathesis rates. The determined reactivity ratios can be used to calculate the instantaneous copolymer composition, thus permitting visualizations of brush distributions. We further synthesized an array of monodisperse polymers (**PLA**^{x}-*ran*-**DME**$^{1-x}$)$_n$ with various grafting densities (x = 1.0, 0.75, 0.5, 0.25) and backbone degrees of polymerization (n = 167, 133, 100, 67, 33). These results demonstrate that ring-opening metathesis copolymerization can be exploited in the context of side chain density/distribution control. Simultaneous control over the density and distribution of grafts via grafting-through ROMP therefore expands the polymer synthetic toolbox, providing new opportunities for designing architecturally complex polymers spanning the linear-to-bottlebrush regimes.[37] We are currently investigating the effects of grafting density variations on the self-assembly and rheological properties of graft polymers.

EXPERIMENTAL SECTION

General Considerations. Norbornene macromonomers **PS**[9] and **PLA**[10] were prepared according to the reported precedures. Norbornenyl diluents **DME**,[38] **DEE**,[39] and **DBE**[40] were prepared by Diels−Alder reactions according to the reported procedures. Grubbs' second-generation catalyst [$(H_2IMes)(PCy_3)(Cl)_2Ru$=CHPh] was provided by Materia, and **G3** was prepared according to the reported

DOI: 10.1021/jacs.7b00791
J. Am. Chem. Soc. 2017, 139, 3896−3903

precedure.[26] CH_2Cl_2 was dried by passing through an activated alumina column. Deuterated solvents were purchased from Cambridge Isotopes Laboratories, Inc. and used as received.

NMR, SEC, and DSC Characterization. Ambient temperature NMR spectra were recorded on a Varian 300, 400, or 500 MHz NMR spectrometer. Chemical shifts (δ) were given in ppm and referenced against residual solvent signals (^1H, ^{13}C). SEC data were collected using two Agilent PLgel MIXED-B 300 × 7.5 mm columns with 10 μm beads, connected to an Agilent 1260 Series pump, a Wyatt 18-angle DAWN HELEOS light scattering detector, and Optilab rEX differential refractive index detector. Online determination of dn/dc assumed 100% mass elution under the peak of interest. The mobile phase was THF. Thermal profiles of polymer samples were obtained using a Hitachi DSC7020 calorimeter with an aluminum reference pan. Following an initial run to erase thermal history (by heating from 25 to 130 °C at a rate of 10 °C/min), sample temperature was maintained at 120 °C in an external oven while the furnace cooled for approximately 20 min. Samples were then removed from the oven, cooled for 45 s on a thermally conductive surface, and then rerun through an identical calorimeter cycle (25−130 °C, 10 °C/min). The reported data were collected on the second heating ramp.

Synthesis of PDMS. A solution of *N*-(hexanoic acid)-*cis*-5-norbornene-*exo*-dicarboximide (6.00 g, 21.6 mmol), alcohol-terminated PDMS (18.1 g, 18.1 mmol, M_n = 1000 g/mol, Gelest), EDC·HCl (5.52 g, 28.8 mmol), and DMAP (222 mg, 1.80 mmol) was prepared in 250 mL of dichloromethane. After being stirred for 20 h under air at room temperature, the organic solution was washed with 1 M HCl (3 × 75 mL), brine (3 × 75 mL), and deionized water (3 × 75 mL). The organic solution was stirred over anhydrous $MgSO_4$ and then filtered, and volatile components were removed under vacuum. The product was filtered through a plug of silica with dichloromethane (2 L), and was dried in vacuo, affording **PDMS** as a colorless oil (18.6 g, 82%). ^1H NMR ($CDCl_3$, 300 MHz) δ 6.28 (s, 2H), 4.20 (dd, 4H), 3.61 (dd, 4H), 3.44 (dt, 10H), 3.27 (t, 4H), 2.33 (t, 2H), 1.59 (m, 9H), 1.31 (m, 6H), 1.21 (d, 1H), 0.88 (t, 4H), 0.52 (td, 4H), 0.07 (s, 104H). M_n (determined by ^1H NMR) = 1280 g/mol.

Standard Procedures for the Determination of Homopolymerization Rate Constants. A 4 mL vial was charged with a flea stir bar and a norbornene monomer (0.025 mmol) in CH_2Cl_2 at 298 K. While stirring vigorously, the polymerization was initiated by adding a CH_2Cl_2 solution of **G3** (0.0125 M, 20 μL, 0.25 μmol) to achieve initial conditions of $[\text{norbornene}]_0$ (0.05 M) and $[\mathbf{G3}]_0$ (0.5 mM). During the course of the reaction, aliquots (~20−50 μL) were extracted at different time points and immediately quenched in a separate vial containing a large excess of ethyl vinyl ether (~0.2 mL) in THF. The quenched reaction mixtures were subsequentially subjected to SEC and ^1H NMR analysis, allowing for the determination of $[\text{norbornene}]_t$. For each homopolymerization experiment, the self-propagation rate constant k_{homo} was determined according to eq 1.

Standard Procedures for the Determination of Copolymerization Reactivity Ratios. A 4 mL vial was charged with a flea stir bar and a CH_2Cl_2 solution of two norbornene monomers (M_1, M_2, each 0.025 mmol) at 298 K. While stirring vigorously, the copolymerization was initiated by adding a CH_2Cl_2 solution of **G3** (0.0125 M, 20 μL, 0.25 μmol) to achieve initial conditions of $[M_1]_0$ (0.05 M), $[M_2]_0$ (0.05 M), and $[\mathbf{G3}]_0$ (0.5 mM). During the course of the reaction, aliquots (~20−50 μL) were extracted at different time points and immediately quenched in a separate vial containing a large excess of ethyl vinyl ether (~0.2 mL) in THF. The quenched reaction mixtures were subsequentially subjected to SEC and ^1H NMR analysis, allowing for the determination of $[M_1]_t$ and $[M_2]_t$. Values of k_{12} and k_{21} were obtained by fitting the experimentally determined kinetic data to the numerical solutions for eqs 2−5 using a MATLAB nonlinear least-squares solver (*lsqcurvefit*) in conjunction with non-stiff differential equation solver (*ode45*).

■ ASSOCIATED CONTENT

Supporting Information

The Supporting Information is available free of charge on the ACS Publications website at DOI: 10.1021/jacs.7b00791.

Spectroscopic characterizations, kinetic details, and curve-fitting codes (PDF)

■ AUTHOR INFORMATION

Corresponding Author

*rhg@caltech.edu

ORCID

Tzu-Pin Lin: 0000-0001-7041-7213

Robert H. Grubbs: 0000-0002-0057-7817

Notes

The authors declare no competing financial interest.

■ ACKNOWLEDGMENTS

This work was supported by the U.S. Department of Energy under award number DE-AR0000683 (ARPA-E program) and by the National Science Foundation under award number CHE-1502616. A.B.C. thanks the U.S. Department of Defense for support through the NDSEG fellowship. A.L.L.-M. thanks the Resnick Sustainability Institute at Caltech for fellowship support. C.M.B. thanks UCSB for funding and the Materials Research Laboratory, a Materials Research Science and Engineering Center (MRSEC) under support from the National Science Foundation (DMR-1121053). C.A.B. thanks the W.M. Keck Foundation for instrumental support.

■ REFERENCES

(1) (a) Hadjichristidis, N.; Pitsikalis, M.; Iatrou, H.; Pispas, S. *Macromol. Rapid Commun.* **2003**, *24*, 979−1013. (b) Sheiko, S. S.; Sumerlin, B. S.; Matyjaszewski, K. *Prog. Polym. Sci.* **2008**, *33*, 759−785. (c) Rzayev, J. *ACS Macro Lett.* **2012**, *1*, 1146−1149. (d) Verduzco, R.; Li, X.; Pesek, S. L.; Stein, G. E. *Chem. Soc. Rev.* **2015**, *44*, 2405−2420. (e) Müllner, M.; Müller, A. H. E. *Polymer* **2016**, *98*, 389−401.

(2) (a) Lecommandoux, S.; Chécot, F.; Borsali, R.; Schappacher, M.; Deffieux, A.; Brûlet, A.; Cotton, J. P. *Macromolecules* **2002**, *35*, 8878−8881. (b) Zhang, B.; Gröhn, F.; Pedersen, J. S.; Fischer, K.; Schmidt, M. *Macromolecules* **2006**, *39*, 8440−8450. (c) Cao, Z.; Carrillo, J.-M. Y.; Sheiko, S. S.; Dobrynin, A. V. *Macromolecules* **2015**, *48*, 5006−5015.

(3) (a) Runge, M. B.; Bowden, N. B. *J. Am. Chem. Soc.* **2007**, *129*, 10551−10560. (b) Hu, M.; Xia, Y.; McKenna, G. B.; Kornfield, J. A.; Grubbs, R. H. *Macromolecules* **2011**, *44*, 6935−6943. (c) Gu, W.; Huh, J.; Hong, S. W.; Sveinbjornsson, B. R.; Park, C.; Grubbs, R. H.; Russell, T. P. *ACS Nano* **2013**, *7*, 2551−2558. (d) Dalsin, S. J.; Hillmyer, M. A.; Bates, F. S. *ACS Macro Lett.* **2014**, *3*, 423−427.

(4) Johnson, J. A.; Lu, Y. Y.; Burts, A. O.; Lim, Y.-H.; Finn, M. G.; Koberstein, J. T.; Turro, N. J.; Tirrell, D. A.; Grubbs, R. H. *J. Am. Chem. Soc.* **2011**, *133*, 559−566.

(5) Li, X.; Prukop, S. L.; Biswal, S. L.; Verduzco, R. *Macromolecules* **2012**, *45*, 7118−7127.

(6) Sun, G.; Cho, S.; Clark, C.; Verkhoturov, S. V.; Eller, M. J.; Li, A.; Pavía-Jiménez, A.; Schweikert, E. A.; Thackeray, J. W.; Trefonas, P.; Wooley, K. L. *J. Am. Chem. Soc.* **2013**, *135*, 4203−4206.

(7) Xu, H.; Sun, F. C.; Shirvanyants, D. G.; Rubinstein, M.; Shabratov, D.; Beers, K. L.; Matyjaszewski, K.; Sheiko, S. S. *Adv. Mater.* **2007**, *19*, 2930−2934.

(8) Bates, C. M.; Chang, A. B.; Schulze, M. W.; Momčilović, N.; Jones, S. C.; Grubbs, R. H. *J. Polym. Sci., Part B: Polym. Phys.* **2016**, *54*, 292−300.

(9) Bates, C. M.; Chang, A. B.; Momčilović, N.; Jones, S. C.; Grubbs, R. H. *Macromolecules* **2015**, *48*, 4967−4973.

DOI: 10.1021/jacs.7b00791
J. Am. Chem. Soc. 2017, 139, 3896−3903

(10) Sveinbjörnsson, B. R.; Weitekamp, R. A.; Miyake, G. M.; Xia, Y.; Atwater, H. A.; Grubbs, R. H. *Proc. Natl. Acad. Sci. U. S. A.* **2012**, *109*, 14332−14336.
(11) Cheng, C.; Khoshdel, E.; Wooley, K. L. *Nano Lett.* **2006**, *6*, 1741−1746.
(12) Daniel, W. F. M.; Burdynska, J.; Vatankhah-Varnoosfaderani, M.; Matyjaszewski, K.; Paturej, J.; Rubinstein, M.; Dobrynin, A. V.; Sheiko, S. S. *Nat. Mater.* **2016**, *15*, 183−189.
(13) Paturej, J.; Sheiko, S. S.; Panyukov, S.; Rubinstein, M. *Science Advances* **2016**, *2*, e1601478.
(14) Noel, A.; Borguet, Y. P.; Wooley, K. L. *ACS Macro Lett.* **2015**, *4*, 645−650.
(15) (a) Peng, S.; Bhushan, B. *RSC Adv.* **2012**, *2*, 8557−8578. (b) Zhang, Q.; Ran, Q.; Zhao, H.; Shu, X.; Yang, Y.; Zhou, H.; Liu, J. *Colloid Polym. Sci.* **2016**, *294*, 1705−1715.
(16) (a) Lipson, J. E. G. *Macromolecules* **1991**, *24*, 1327−1333. (b) Rouault, Y.; Borisov, O. V. *Macromolecules* **1996**, *29*, 2605−2611. (c) Saariaho, M.; Subbotin, A.; Szleifer, I.; Ikkala, O.; ten Brinke, G. *Macromolecules* **1999**, *32*, 4439−4443. (d) Elli, S.; Ganazzoli, F.; Timoshenko, E. G.; Kuznetsov, Y. A.; Connolly, R. *J. Chem. Phys.* **2004**, *120*, 6257−6267.
(17) Ohno, S.; Matyjaszewski, K. *J. Polym. Sci., Part A: Polym. Chem.* **2006**, *44*, 5454−5467.
(18) Matsuda, M.; Satoh, K.; Kamigaito, M. *Macromolecules* **2013**, *46*, 5473−5482.
(19) (a) Bielawski, C. W.; Grubbs, R. H. *Prog. Polym. Sci.* **2007**, *32*, 1−29. (b) Leitgeb, A.; Wappel, J.; Slugovc, C. *Polymer* **2010**, *51*, 2927−2946. (c) Sutthasupa, S.; Shiotsuki, M.; Sanda, F. *Polym. J.* **2010**, *42*, 905−915. (d) Martinez, H.; Ren, N.; Matta, M. E.; Hillmyer, M. A. *Polym. Chem.* **2014**, *5*, 3507−3532.
(20) (a) Lutz, J.-F.; Ouchi, M.; Liu, D. R.; Sawamoto, M. *Science* **2013**, *341*, 1238149. (b) Chang, A. B.; Miyake, G. M.; Grubbs, R. H. In *Sequence-Controlled Polymers: Synthesis, Self-Assembly, and Properties*; Lutz, J.-F., Meyer, T. Y., Ouchi, M., Sawamoto, M., Eds.; ACS Symposium Series *1170*;American Chemical Society: Washington, DC, 2014; pp 161−188.
(21) (a) Al Samak, B.; Carvill, A. G.; Rooney, J. J.; Thompson, J. M. *Chem. Commun.* **1997**, 2057−2058. (b) Elling, B. R.; Xia, Y. *J. Am. Chem. Soc.* **2015**, *137*, 9922−9926.
(22) (a) Sutthasupa, S.; Shiotsuki, M.; Masuda, T.; Sanda, F. *J. Am. Chem. Soc.* **2009**, *131*, 10546−10551. (b) Jeong, H.; John, J. M.; Schrock, R. R. *Organometallics* **2015**, *34*, 5136−5145. (c) Jang, E. S.; John, J. M.; Schrock, R. R. *ACS Cent. Sci.* **2016**, *2*, 631−636.
(23) (a) Jha, S.; Dutta, S.; Bowden, N. B. *Macromolecules* **2004**, *37*, 4365−4374. (b) Xia, Y.; Olsen, B. D.; Kornfield, J. A.; Grubbs, R. H. *J. Am. Chem. Soc.* **2009**, *131*, 18525−18532. (c) Li, Z.; Zhang, K.; Ma, J.; Cheng, C.; Wooley, K. L. *J. Polym. Sci., Part A: Polym. Chem.* **2009**, *47*, 5557−5563.
(24) (a) Lu, H.; Wang, J.; Lin, Y.; Cheng, J. *J. Am. Chem. Soc.* **2009**, *131*, 13582−13583. (b) Zhang, H.; Zhang, Z.; Gnanou, Y.; Hadjichristidis, N. *Macromolecules* **2015**, *48*, 3556−3562.
(25) Moatsou, D.; Hansell, C. F.; O'Reilly, R. K. *Chem. Sci.* **2014**, *5*, 2246−2250.
(26) Love, J. A.; Morgan, J. P.; Trnka, T. M.; Grubbs, R. H. *Angew. Chem., Int. Ed.* **2002**, *41*, 4035−4037.
(27) Trzaskowski, B.; Grela, K. *Organometallics* **2013**, *32*, 3625−3630.
(28) (a) Mayo, F. R.; Lewis, F. M. *J. Am. Chem. Soc.* **1944**, *66*, 1594−1601. (b) Mayo, F. R.; Walling, C. *Chem. Rev.* **1950**, *46*, 191−287.
(29) Fineman, M.; Ross, S. D. *J. Polym. Sci.* **1950**, *5*, 259−262.
(30) Kelen, T.; Tüdös, F. *J. Macromol. Sci., Chem.* **1975**, *9*, 1−27.
(31) Jaacks, V. *Makromol. Chem.* **1972**, *161*, 161−172.
(32) Odian, G. *Principles of Polymerization*, 4th ed.; John Wiley & Sons, Inc.: Hoboken, NJ, 2004.
(33) Radzinski, S. C.; Foster, J. C.; Chapleski, R. C.; Troya, D.; Matson, J. B. *J. Am. Chem. Soc.* **2016**, *138*, 6998−7004.
(34) (a) Börner, H. G.; Duran, D.; Matyjaszewski, K.; da Silva, M.; Sheiko, S. S. *Macromolecules* **2002**, *35*, 3387−3394. (b) Lee, H.-i.; Matyjaszewski, K.; Yu, S.; Sheiko, S. S. *Macromolecules* **2005**, *38*, 8264−8271.
(35) Singh, N.; Tureau, M. S.; Epps, T. H., III *Soft Matter* **2009**, *5*, 4757−4762.
(36) The presence of two T_g values suggests either blocky copolymerization (inconsistent with our kinetic data) or microphase separation of **PS**-functionalized and **DBE**-functionalized segments. The observation of a single T_g supports random copolymerization as predicted.
(37) Bates, C. M.; Bates, F. S. *Macromolecules* **2017**, *50*, 3−22.
(38) Hickey, S. M.; Ashton, T. D.; Khosa, S. K.; Robson, R. N.; White, J. M.; Li, J.; Nation, R. L.; Yu, H. Y.; Elliott, A. G.; Butler, M. S.; Huang, J. X.; Cooper, M. A.; Pfeffer, F. M. *Org. Biomol. Chem.* **2015**, *13*, 6225−6241.
(39) Windmon, N.; Dragojlovic, V. *Green Chem. Lett. Rev.* **2008**, *1*, 155−163.
(40) Park, J.-S.; Oh, H.-C.; Park, Y.-S.; Woo, J.-W. *Adv. Mater. Res. (Durnten-Zurich, Switz.)* **2011**, *421*, 136−139.

DOI: 10.1021/jacs.7b00791
J. Am. Chem. Soc. 2017, 139, 3896−3903